Finite-temperature theory of local-environment effects in Fe-Ni alloys

Y. Kakehashi
Department of Physics, Hokkaido Institute of Technology, Teine-Maeda, Nishi-ku, Sapporo 006, Japan
(Received 10 June 1987; revised manuscript received 16 February 1988)

Magnetic properties of Fe-Ni alloys have been investigated for both fcc and bcc structures on the basis of the finite-temperature theory of local-environment effects (LEE). The temperature and concentration dependencies of various local moments, susceptibilities, and the internal-field distribution function have been calculated. The results are analyzed from the viewpoint of the LEE. The magnetic phase diagram obtained explains the experimental results well; the bcc alloys show a stable ferromagnetism while the fcc has a ferromagnetic instability at about 65 at. % Fe. In particular, the spin-glass state in the fcc phase is theoretically obtained for the first time on the basis of the itinerant-electron model. It is shown to be a new type of itinerant-electron spin glass which arises from the nonlinearity of the magnetic couplings between Fe local moments. The theory predicts also an asymmetric divergence of the high-field susceptibility around the ferromagnetic instability in the fcc lattice.

I. INTRODUCTION

Local-environment effects (LEE) are important to describe the magnetic behavior of Fe-Ni alloys in the vicinity of the ferromagnetic instability where the energy difference between various magnetic states with local moments (LM) is very small. We therefore developed in a previous paper[1] (which is hereafter referred to as I), a theory of LEE at finite temperatures. The theory self-consistently takes into account the number of nearest-neighbor atomic and magnetic configurations ($2^{12}\times 2^{12}=16\,771\,216$) for the fcc structure at finite temperatures by using the method of the distribution function[2,3] and the static approximation to the two-field functional-integral method.[4-6] Applying this theory to Fe-Ni alloys we have shown that a rapid but continuous decrease in the curve of magnetization versus concentration[7] is obtained by taking account of the large fluctuation of Fe local moments with respect to the atomic configuration. This large fluctuation implies a broad distribution of Fe LM's, and causes a broad internal-field distribution near the critical concentration c^* of the ferromagnetic instability, in agreement with experiment.[8-14] The downward deviation of the magnetization curves from the $S=\frac{1}{2}$ Brillouin curve was shown to be caused by the collapse of the strong ferromagnetism and the randomness of the alloys.

Since we published paper I, there have been several attempts to describe the ground-state properties on the basis of first-principle band calculations. In particular, Williams and Kübler[15] performed compound calculations. They showed that a decrease of the magnetization at the Invar concentration is possible in the fcc lattice. Johnson *et al.*[16] calculated the density of states for $Fe_{65}Ni_{35}$ by using the Korringa-Kohn-Rostoker coherent-potential approximation (KKR-CPA) method. They clarified the details of the band structure. Although these calculations are an important step towards the complete understanding of the magnetism of Fe-Ni alloys, the fluctuations of the LM's with respect to the atomic configuration and self-consistency for the LM configuration are apparently missing. Thus it is not possible to use these methods to describe the rapid but *continuous* decrease of the magnetization in the ground state, the internal-field distribution function, and other magnetic anomalies near c^*. One has to develop a method which self-consistently takes account of LEE to progress in the band theory of magnetism in alloys.

In the present paper we investigate various magnetic quantities in Fe-Ni alloys in more detail using our finite-temperature theory of LEE. This work has several motivations.

First, theoretical examinations have recently been made on the validity of the two-field static approximation in the degenerate-Hubbard-band model.[17,18] In particular, it has been shown that the five-equivalent-band model used in paper I does not simply mean five times the single-band model, but is a significant model which takes account of the effects of degeneracy and Hund's rule coupling.[18] This encourages further numerical calculations based on the theory of LEE. Moreover, a new expression for the amplitude of the LM's $\langle \mathbf{m}^2 \rangle$, which takes account of a quantum effect, was obtained.[18] Since the quantum effects strongly enhance the amplitude of the LM's, it is desirable to investigate again LEE on the amplitude of the LM. Such investigations are important, in particular, for the Fe-Ni alloys because the amplitude of the LM is the most important physical parameter in the Invar problem.[19]

Second, Takahashi *et al.*[20] have quite recently reported that a spin-glass state exists at low temperatures in $Fe_{65}Ni_{35}$ alloys. The Fe-Ni binary alloys undergo the martensitic transformation at more than 65 at. % Fe. Thus they investigated[21] quasi-Fe-Ni fcc alloys, i.e., $(Fe_cNi_{1-c})_{92}C_8$ alloys ($0.6<c<0.9$), and deduced a magnetic phase diagram showing the spin-glass phase boundary in the temperature-concentration plane. Therefore, it is worth investigating theoretically, the possibility of the

existence of the spin-glass state in the Fe-Ni concentrated alloys.

A spin-glass theory for itinerant-electron systems has been developed by Hertz[22] on the basis of the functional-integral method in order to understand the relation between the Kondo impurity and the spin-glass state at low concentrations. He assumed linear and long-range pair interactions (i.e., Gaussian-type interactions) and the dilute alloys. On the other hand, our theory of LEE (Ref. 1) treats concentrated alloys and the nonlinear-pair-energy functional between nearest-neighbor sites. Thus our theory is complementary to the Hertz theory and is apparently suitable for the present purpose.

Third, susceptibilities and magnetic properties in the bcc phase have not yet been investigated on the basis of the theory of LEE. The results of the calculations should be published in order to clarify the consistency of the theory and its limitation.

In Sec. II we briefly summarize the method of the calculations. Details of the theory have been presented in Refs. 23 and 1. We present in Sec. III a magnetic phase diagram which includes the bcc phase as well as the fcc. It is shown that a spin-glass state is possible after the disappearance of the ferromagnetism. It is a typical itinerant-electron spin glass based on a new formation mechanism. A preliminary report for this point has been published previously.[24] Details of LEE on local moments are given in Sec. IV. The concentration and temperature dependencies of the amplitude of the LM are presented there. Better agreement with experiment is obtained for the internal-field distribution function.

In Sec. V the results for the high-field susceptibility and the paramagnetic susceptibility are presented. Asymmetric divergence of the high-field susceptibility around the critical concentration is found for the fcc structure. Finally, we summarize our results in Sec. VI.

II. FINITE-TEMPERATURE THEORY OF LEE

In this section we briefly review the finite-temperature theory of LEE. A full description of the theory has been presented in previous papers.[1,23]

We adopt the degenerate-band Hubbard model with Hund's rule coupling, and apply the static approximation to the two-field functional-integral method.[18,23] The thermal average of a LM at site i is then expressed as a classical average of the field variable ξ_i on the same site with respect to the free-energy functional $E(\xi)$ of a one-electron system with the fictitious fields $\xi=(\xi_1,\xi_2,\ldots,\xi_N)$ acting on the N different sites.

Next, an effective medium $\propto\sigma^{-1}$, which describes the effect of the random potentials and the thermal spin fluctuations on average, is inserted into the diagonal part of the one-electron Hamiltonian in $E(\xi)$. The deviation from the effective medium is expanded with respect to sites in the energy functional $E(\xi)$. To zeroth order one uses the effective medium only. The first-order correction consists of the sum of the energy functionals $E_i(\xi_i)$ of the "impurity" on site i embedded in the effective medium. The next term forms the pair interactions $\sum_{(i,j)}\Phi_{ij}(\xi_i,\xi_j)$. Here $\Phi_{ij}(\xi_i,\xi_j)$ is the pair-energy functional between sites i and j [see Eq. (2.13) of Ref. 23]. We take account of the nearest-neighbor (NN) pair interactions only, and neglect those between more distant atoms. Moreover, all higher-order terms are neglected in the present theory. Next we replace the surrounding field variables by effective Ising spins in the thermal average of a LM by making use of a decoupling approximation which is correct up to the second moment. Finally the local magnetic moment on site 0 is expressed within the molecular-field approximation as follows [see Eqs. (2.24) and (2.25) of Ref. 23].

$$\langle m_0\rangle\equiv\frac{\int d\xi\,\xi e^{-\beta\Psi(\xi)}}{\int d\xi\, e^{-\beta\Psi(\xi)}}\ , \tag{2.1}$$

$$\Psi(\xi)=E_0(\xi)+\sum_{i\neq0}^{z}\Phi_{0i}(\xi)-\sum_{i\neq0}^{z}\Phi_{0i}^{\mathrm{ex}}(\xi)\frac{\langle m_i\rangle}{x_i}\ . \tag{2.2}$$

Here β denotes the inverse temperature, z being the number of the nearest neighbors. $\langle m_i\rangle$ in Eq. (2.2) is the average LM on the neighboring site i. A single-site amplitude x_i is defined by

$$x_i^2=\int d\xi\,\xi^2\exp[-\beta E_i(\xi)]\Big/\int d\xi\exp[-\beta E_i(\xi)]\ .$$

The atomic and exchange pair-energy functionals $\Phi_{0i}(\xi)$ and $\Phi_{0i}^{\mathrm{ex}}(\xi)$ are defined by

$$\overline{\Phi}_{0i}(\xi)=\tfrac{1}{2}\sum_{\nu=\pm}\Phi_{0i}(\xi,\nu x_i)\ , \tag{2.3}$$

$$\Phi_{0i}^{\mathrm{ex}}(\xi)=-\tfrac{1}{2}\sum_{\nu=\pm}\nu\Phi_{0i}(\xi,\nu x_i)\ . \tag{2.4}$$

Equation (2.1) clearly shows that the central local moment in an effective medium is determined by the surrounding atomic and magnetic configurations $\{\gamma_i\}$ and $\{\langle m_i\rangle\}$ via the energy functional $\Psi(\xi)$, where γ_i denotes the type of atom on a surrounding site i (see Fig. 1). The local moments $\{\langle m_i\rangle\}$ are determined in principle by solving coupled equations of the type (2.1) obtained on each site.

In disordered alloys the random configuration of sur-

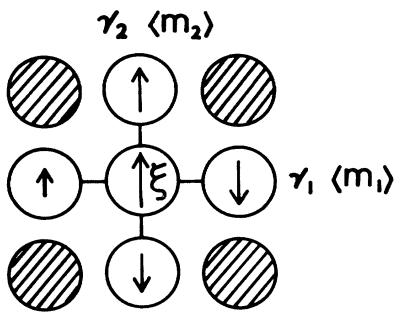

FIG. 1. Local moment with a local environment in the effective medium. Flexible local moment ξ is coupled to the surrounding atoms $\{\gamma_i\}$ and local moments $\{\langle m_i\rangle\}$ via the atomic ($\overline{\Phi}_{0i}$) and exchange (Φ_{0i}^{ex}) pair-energy functionals.

rounding atoms produces various local magnetic states at the central site via Eq. (2.1), and therefore a local-moment distribution $g_\alpha^{(1)}(m)$. Here α denotes the type of atom at the central site. The distribution is determined from Eq. (2.1) once we know the distribution of surroundings LM's $\{\langle m_i\rangle\}$. Since the latter should have the same form as the central one we obtain an integral equation for $g_\alpha^{(1)}(m)$. Further approximations lead to the self-consistent equations for the average LM of the atom α ($[\langle m_\alpha\rangle]_c$) and the configurational average of the square of the LM ($[\langle m_\alpha\rangle^2]_c$):

$$x_\alpha u_\alpha=[\langle m_\alpha\rangle]_c \ , \tag{2.5a}$$

$$x_\alpha^2 v_\alpha^2=[\langle m_\alpha\rangle^2]_c \ , \tag{2.5b}$$

$$[\langle m_\alpha\rangle^i]_c=\sum_{n=0}^{z}\Gamma(n,z,p_a^{\alpha\alpha})[\langle m_\alpha\rangle_n^i]_c, \quad (i=1,2) \tag{2.6}$$

$$[\langle m_\alpha\rangle_n^i]_c=\sum_{k=0}^{n}\sum_{l=0}^{z-n}\Gamma(k,n,q_{\alpha+})\Gamma(l,z-n,q_{\bar\alpha+}) \times(\langle\xi_\alpha\rangle_{nkl})^i \ , \tag{2.7}$$

$$q_{\alpha\pm}=\frac{1}{2}\left[1\pm\frac{u_\alpha}{v_\alpha}\right] . \tag{2.8}$$

Here $\langle\ \rangle$ ($[\ ]_c$) denotes the thermal (configurational) average. The site index i in x_i has been replaced by the type of atom on site i.

Equations (2.5a) and (2.5b) define unknown parameters u_α and v_α. Equation (2.6) shows that the averaged LM's $[\langle m_\alpha\rangle]_c$ are obtained by averaging the LM's $[\langle m_\alpha\rangle_n]_c$ over the NN atomic configuration described by the binomial distribution function $\Gamma(n,z,p_a^{\alpha\alpha})$ defined by

$$[z!/n!(z-n)!](p_a^{\alpha\alpha})^n(1-p_a^{\alpha\alpha})^{z-n} \ .$$

Here $p_a^{\alpha\alpha}$ is the probability of finding an atom α at a neighboring site of an atom α, and is given in terms of Cowley's atomic short-range order parameter τ as $p_a^{\alpha\alpha}=c_\alpha+(1-c_\alpha)\tau$, c_α being the concentration of the atom α. Equation (2.7) is concerned with the LM's in a given NN atomic configuration, which are averaged over the local moment distribution at the surrounding sites. $q_{\alpha+}$ ($q_{\alpha-}$) in Eq. (2.8) means the probability that the fictitious spin on atom α with magnitude v_α is in the up (down) direction. $\langle\xi_\alpha\rangle_{nkl}$ in Eq. (2.7) is the local moment of an atom of type α at the central site when k of the fictitious spins among the surrounding n atoms of type α point up, and in addition, l spins of the remaining z-n atoms of type $\bar\alpha$ also point up:

$$\langle\xi_\alpha\rangle_{nkl}=\int p_{\alpha nkl}(\xi)\xi d\xi \ , \tag{2.9}$$

$$p_{\alpha nkl}(\xi)\equiv\frac{e^{-\beta\Psi_{\alpha nkl}(\xi)}}{\int d\xi\, e^{-\beta\Psi_{\alpha nkl}(\xi)}} \ , \tag{2.10}$$

$$\Psi_{\alpha nkl}(\xi)=E_\alpha(\xi)+n\bar\Phi_{\alpha\alpha}(\xi)+(z-n)\bar\Phi_{\alpha\bar\alpha}(\xi) -(2k-n)\Phi_{\alpha\alpha}^{\rm ex}(\xi)v_\alpha-(2l-z+n)\Phi_{\alpha\bar\alpha}^{\rm ex}(\xi)v_{\bar\alpha} \ . \tag{2.11}$$

Here the site indices i and j in the impurity energy and pair-energy functionals in Eq. (2.11) have been replaced by the type of atoms on the sites.

As we have mentioned before, Eqs. (2.5a) and (2.5b) determine $[\langle m_\alpha\rangle]_c$ and $[\langle m_\alpha\rangle^2]_c$ when the medium $\{\mathcal{L}_\sigma^{-1}\}$ is given, since the energy functionals $E_\alpha(\xi)$, $\bar\Phi_{\alpha\gamma}(\xi)$, and $\Phi_{\alpha\gamma}^{\rm ex}(\xi)$ in Eq. (2.11) are functionals of the medium $\{\mathcal{L}_\sigma^{-1}\}$. We determine the effective medium $\mathcal{L}_\sigma^{-1}$ so that the single-site electron scattering from the medium disappears [see Eq. (2.40) of Ref. 23]:

$$\sum_\alpha c_\alpha\sum_{\nu=\pm}\frac{1}{2}\left[1+\nu\frac{[\langle\xi_\alpha\rangle]_c}{([\langle\xi_\alpha^2\rangle]_c)^{1/2}}\right]|r_\alpha|^2G_{\alpha\sigma}(\omega,\nu([\langle\xi_\alpha^2\rangle]_c)^{1/2},\mathcal{L}_\sigma^{-1})=F(\mathcal{L}_\sigma^{-1}) \ . \tag{2.12}$$

This is called the coherent-potential approximation (CPA). Here $[\langle\xi_\alpha^i\rangle]_c$ ($i=1,2$) is defined by

$$[\langle\xi_\alpha^i\rangle]_c=\sum_{n=0}^{z}\Gamma(n,z,p_a^{\alpha\alpha})\sum_{k=0}^{n}\sum_{l=0}^{z-n}\Gamma(k,n,q_{\alpha+})\Gamma(l,z-n,q_{\alpha+})\langle\xi_\alpha^i\rangle_{nkl} \ , \tag{2.13}$$

$$\langle\xi_\alpha^i\rangle_{nkl}=\int\xi^i p_{\alpha nkl}(\xi)d\xi \ . \tag{2.14}$$

$G_{\alpha\sigma}(\omega,\xi,\mathcal{L}_\sigma^{-1})$ in Eq. (2.12) is the one-electron Green function at an impurity site occupied by an atom of type α in spin state σ with the field variable ξ,

$$G_{\alpha\sigma}(\omega,\xi,\mathcal{L}_\sigma^{-1})=\frac{1}{|r_\alpha|^2}\left[\frac{\omega-w_\alpha(\xi)+\mu+\frac{1}{2}\tilde J_\alpha\xi\sigma}{|r_\alpha|^2} -\mathcal{L}_\sigma^{-1}+F(\mathcal{L}_\sigma^{-1})^{-1}\right]^{-1} , \tag{2.15}$$

where $|r_\alpha|^2$ is the off-diagonal factor in the CPA, $w_\alpha(\xi)$ is the charge potential of atom α, μ is the chemical potential, and $\tilde J_\alpha$ denotes the effective exchange energy parameter of atom α. $F(\propto\sigma^{-1})$ is the coherent electron Green function of spin σ,

$$F(\mathcal{L}_\sigma^{-1})=\int\frac{\rho(\varepsilon)\,d\varepsilon}{\mathcal{L}_\sigma^{-1}-\varepsilon} \ , \tag{2.16}$$

where $\rho(\varepsilon)$ is the density of states (DOS) for an energy

band of the pure metal with no interaction. Note that $G_{\alpha\sigma}$ and F do not depend on the orbital because we have adopted the fivefold equivalent band model. Equations (2.5a), (2.5b), and (2.12) have to be solved self-consistently together with the equation for the determination of charge potentials which appear in $E_\alpha(\xi)$, $G_{\alpha\sigma}$, etc.

The distributions of the LM at atom α, the amplitude of LM $(\langle m_\alpha^2 \rangle)^{1/2}$, and the internal-field distribution seen by nuclei of atom α are calculated from the following expressions (see Appendix of Ref. 25):

$$\begin{bmatrix} g_\alpha^{(1)}(M) \\ g_\alpha^{(2)}(M) \\ P_\alpha(H) \end{bmatrix} = \sum_{n=0}^{z} \Gamma(n,z,p_a^{\alpha\alpha}) \sum_{k=0}^{n} \sum_{l=0}^{z-n} \Gamma(k,n,q_{\alpha+}) \Gamma(l,z-n,q_{\bar{\alpha}+}) \begin{Bmatrix} \delta(M-\langle \xi_\alpha \rangle_{nkl}) \\ \delta(M-(\langle m_\alpha^2 \rangle_{nkl})^{1/2}) \\ \delta(H-H_{ankl}) \end{Bmatrix} , \tag{2.17}$$

where

$$\langle m_\alpha^2 \rangle_{nkl} = 3n_\alpha - \tfrac{3}{10} n_\alpha^2 + \tfrac{11}{10} (\langle \xi_\alpha^2 \rangle_{nkl} - 2/\beta \tilde{J}_\alpha) , \tag{2.18}$$

$$H_{ankl} = a_\alpha \langle \xi_\alpha \rangle_{nkl} + (2k-l) b_{\alpha\alpha} x_\alpha v_\alpha + (2l-z+n) b_{\alpha\bar{\alpha}} x_{\bar{\alpha}} v_{\bar{\alpha}} . \tag{2.19}$$

We have assumed here a phenomenological expression for the internal field acting on atom i,

$$H_i = a_i \langle m_i \rangle + \sum_{j=1}^{z} b_{ij} \langle m_j \rangle , \tag{2.20}$$

where $\langle m_j \rangle$ is a local moment at the neighboring site j. All results for $g_\alpha^{(1)}(M)$, $g_\alpha^{(2)}(M)$, and $P_\alpha(H)$ are shown by histograms in the following sections.

III. PHASE DIAGRAM AND ITINERANT-ELECTRON SPIN GLASS

We adopted the following set of input parameters for both bcc and fcc lattices to obtain a reasonable critical concentration of the ferromagnetic instability:

$$n_{\mathrm{Fe}} = 7.05, \quad W_{\mathrm{Fe}} = 0.45 \text{ Ry}, \quad \tilde{J}_{\mathrm{Fe}} = 0.0700 \text{ Ry} ,$$
$$n_{\mathrm{Ni}} = 9.00, \quad W_{\mathrm{Ni}} = 0.35 \text{ Ry}, \quad \tilde{J}_{\mathrm{Ni}} = 0.0983 \text{ Ry} .$$

Here n_α, W_α, and $\tilde{J}_\alpha$ are the electron number, d-band width, and effective exchange energy parameter, respectively. These parameters lead to a magnetization of $2.23\mu_B$ at $T=0$ for bcc Fe, and a local magnetization $1.54\mu_B$ for paramagnetic fcc Fe at $T=0$. The former should be compared with the experimental value $2.216\mu_B$.[26] The latter is consistent with the theoretical value $1.87\mu_B$ in the KKR-CPA.[27] The ground-state magnetization $0.62\mu_B$ of Ni in the present calculation is in good agreement with the experimental value $0.615\mu_B$.[26] The model DOS $\rho(\varepsilon)$ are given in the inset of Fig. 2.

A measure of the magnitude of magnetic coupling between atoms α and γ is given by the effective exchange energy $\mathcal{J}_{\alpha\gamma}$ defined by

$$\mathcal{J}_{\alpha\gamma} = -\tfrac{1}{4} \sum_{\lambda=\pm} \sum_{\mu=\pm} \lambda\mu \Phi_{\alpha\gamma}(\lambda x_\alpha, \mu x_\gamma) = \tfrac{1}{2} \sum_{\lambda=\pm} \lambda \Phi_{\alpha\gamma}^{\mathrm{ex}}(\lambda x_\alpha) . \tag{3.1}$$

We note that Eq. (2.1) reduces to the following localized model when the medium is chosen to be spin independent and the amplitude fluctuation is neglected:

$$\langle s_0 \rangle = \frac{\langle m_0 \rangle}{x_0} = \frac{\sum_{s_0=\pm} s_0 \exp\left[-\beta \left[\sum_{j\neq 0}^{z} \mathcal{J}_{0j} \langle s_j \rangle\right] s_0\right]}{\sum_{s_0=\pm} \exp\left[-\beta \left[\sum_{j\neq 0} \mathcal{J}_{0j} \langle s_j \rangle\right] s_0\right]} . \tag{3.2}$$

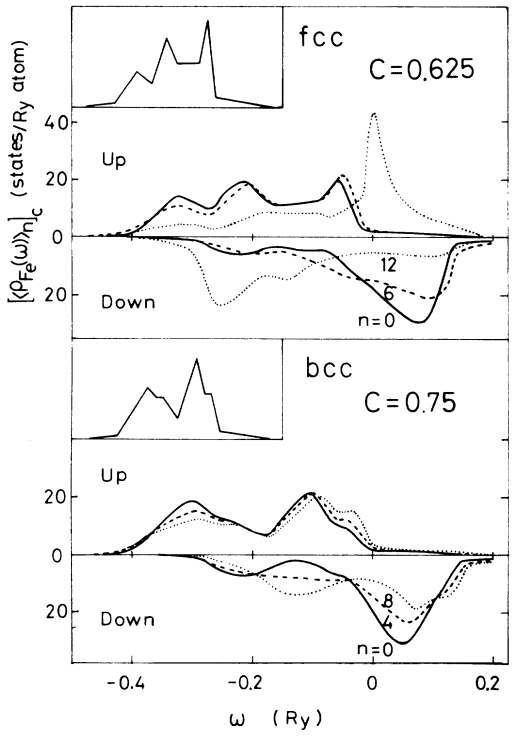

FIG. 2. The fcc and bcc local density of states for Fe in various environments specified by n (the number of Fe nearest neighbors) at $T=150$ K. The values of C denote the Fe concentration here and in the following figures. The insets show the model density of states used in the calculations.

The coupling $\mathcal{J}_{\alpha\gamma}$ reduces to the Anderson superexchange interaction for a half-filled case in the insulator limit[28,29].

Calculated $\mathcal{J}_{\alpha\gamma}$ are shown in Fig. 3. The interactions in the fcc lattice qualitatively agree with those in I. The most important difference between bcc and fcc is seen in the Fe-Fe interactions; $\mathcal{J}_{\mathrm{FeFe}}$ is ferromagnetic in bcc, while it rather shows the antiferromagnetic couplings. The Fe-Ni couplings are enhanced by changing the structure from fcc to bcc.

The magnetic phase diagram in the present theory is shown in Fig. 4(a). fcc Fe is considered to show type I antiferromagnetic structure in which the LM are parallel to each other in a (001) plane but they vary alternately along a [001] axis. Thus one has to calculate the Néel temperatures in Fe-Ni binary alloys to complete the phase diagram. This has not yet been performed because of its laborious nature.

When the Fe concentration increases, the Curie temperatures in the fcc alloys rise. This is explained by a simple replacement of the ferromagnetic couplings $\mathcal{J}_{\mathrm{NiNi}}$ by the stronger ferromagnetic couplings $\mathcal{J}_{\mathrm{FeNi}}$ with increasing Fe concentration. The Curie temperature shows a maximum at about 30 at. % Fe, and finally disappears at 70 at. % Fe because the weak Fe-Fe interactions lower the molecular field acting on the LM.

The present choice of parameters leads to a spin-glass state ($[\langle m_i \rangle]_c = 0$ and $[\langle m_i \rangle^2]_c \neq 0$) in the fcc lattice. Ishio, Nushiro, and Takahashi[21] have quite recently determined the magnetic phase diagram of the fcc $(\mathrm{Fe}_c\mathrm{Ni}_{1-c})_{92}\mathrm{C}_8$ $(0.6 < c < 0.9)$ alloys which simulate the fcc Fe_c-Ni_{1-c} $(0.65 < c < 1.0)$ binary alloys. The spin-glass temperature T_g decreases with increasing Fe concentration and disappears at $c = 0.9$ as shown in Fig. 4(b). The result shows a good correspondence with our phase diagram in Fig. 4(a). In the present calculations we have neglected the transverse spin fluctuations, and have adopted a molecular-field approximation. This is probably the reason why the calculated T_g are much higher than the experimental values. It is quite interesting, in connection with this point, to see a spin glass in amorphous Fe alloys in which the frustration of spins on the fcc lattice disappears so that the molecular-field approximation becomes better. Recent investigations show that $T_g \approx 110$ K in amorphous $\mathrm{Fe}_{93}\mathrm{Zr}_7$ alloys[31] and $T_g \approx 120$ K in amorphous $\mathrm{Fe}_{90}\mathrm{La}_{10}$ alloys,[32] which are several times as large as those in $(\mathrm{Fe}_c\mathrm{Ni}_{1-c})_{92}\mathrm{C}_8$ alloys, and consistent with our results in magnitude.

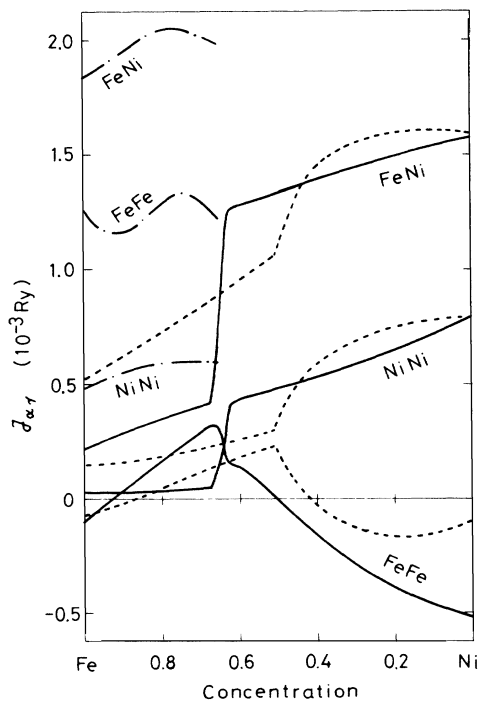

FIG. 3. Exchange pair interactions $\mathcal{J}_{\alpha\gamma}$ for the fcc (solid curves) and bcc (dotted-dashed curves) structures at $T = 150$ K. The fcc results at 900 K are also shown by dashed curves.

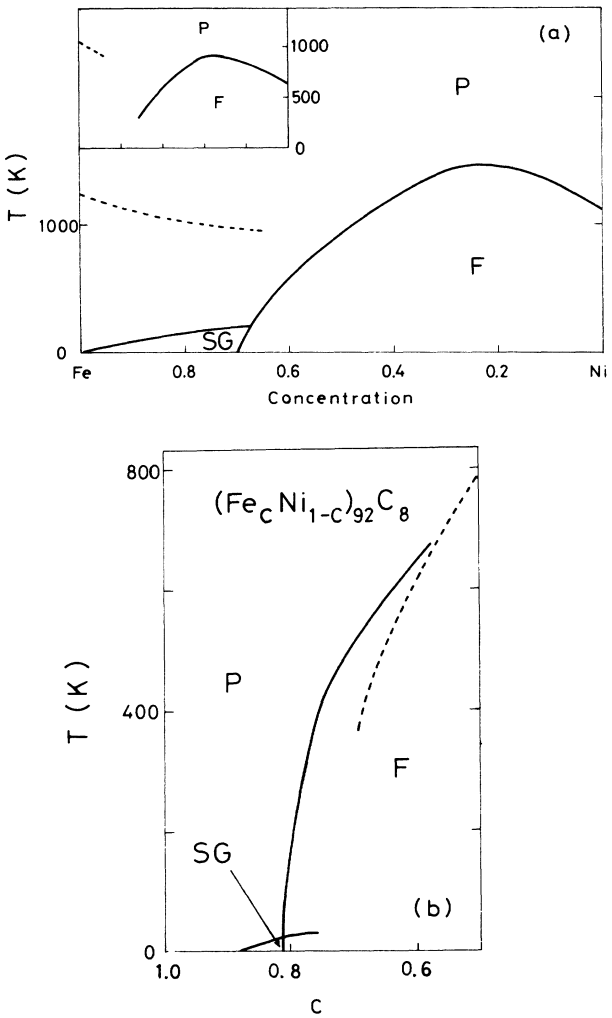

FIG. 4. (a) Calculated magnetic phase diagram showing the ferromagnetic (F), spin-glass (SG), and paramagnetic (P) states. The Curie temperatures for the bcc structure are shown by dashed curve. The inset shows the experimental result (Ref. 30). (b) The experimental phase diagram for $(\mathrm{Fe}_c\mathrm{Ni}_{1-c})_{92}\mathrm{C}_8$ by Ishio *et al.* (Ref. 21), which shows the existence of the spin-glass state in the fcc lattice. The dashed curve shows the Curie temperatures for the binary Fe-Ni alloys (Ref. 30).

In the following we show that the spin-glass state in Fe-Ni alloys is formed by a new mechanism. As seen from Eq. (3.2), the present theory gives the well-known spin-glass temperature T_g of the molecular-field approximation,[33]

$$T_g^2=\tfrac{1}{2}z\{\, c_A\mathcal{J}_{AA}^2+c_B\mathcal{J}_{BB}^2 +[(c_A\mathcal{J}_{AA}^2-c_B\mathcal{J}_{BB}^2)^2+4c_Ac_B\mathcal{J}_{AB}^4]^{1/2}\}\ , \quad (3.3)$$

if we neglect the amplitude fluctuations due to the atomic configuration, and the temperature dependence of $\mathcal{J}_{\alpha\gamma}$. This is nothing else but a localized model, and explains well the existence of the spin glass in Ni-Mn alloys since $\mathcal{J}_{\mathrm{NiNi}}>0$, $\mathcal{J}_{\mathrm{NiMn}}>0$, and $\mathcal{J}_{\mathrm{MnMn}}<0$.[33,34] However, all the exchange interactions $\mathcal{J}_{\alpha\gamma}$ in Fe-Ni alloys are positive in the spin-glass regime as shown in Fig. 3. Therefore, the spin glasses in Fe-Ni alloys are not explained by the localized model. We have to take account of LEE on the amplitude of the LM and the anomalous magnetic couplings between Fe LM to explain the presence of the spin glass.

Figure 5(a) shows the field-variable dependence of the magnetic couplings. The curves do not sensitively depend on the temperature. As seen from Eq. (2.2), $\bar{\Phi}_{\alpha\gamma}(\xi)$ $[-\Phi_{\alpha\gamma}^{\mathrm{ex}}(\xi)]$ means the atomic (exchange) pair-energy contribution to the adiabatic energy $\Psi(\xi)$ of a flexible central LM ξ when the neighboring LM with the amplitude x_γ points up. If the pair interactions follow the Gaussian form, the ξ dependence of $\Phi_{\alpha\gamma}^{\mathrm{ex}}(\xi)$ should be linear and there is no anomaly in the vicinity of the ferromagnetic instability. However, the exchange energy functional $\Phi_{\mathrm{FeFe}}^{\mathrm{ex}}(\xi)$ in the fcc structure shows an S-shape curve as seen in Fig. 5. This implies that Fe LM's, with the average amplitude ($\langle\xi^2\rangle^{1/2}$) less than about $1.7\mu_B$, couple antiferromagnetically to the neighboring Fe LM's, while the Fe LM's with the amplitude more than $1.7\mu_B$ couple ferromagnetically to the surrounding Fe LM's. Since the pair-energy functionals $\bar{\Phi}_{\mathrm{FeFe}}(\xi)$ and $\bar{\Phi}_{\mathrm{FeNi}}(\xi)$ show the downward and upward convex curves, respectively, the amplitude of the central LM varies from $2.6\mu_B$ to $1.5\mu_B$ with increasing the number of Fe NN. This means that the Fe LM's with a small number of Fe NN show the ferromagnetic coupling to the neighboring Fe LM, while the Fe LM with a large number of Fe NN show the antiferromagnetic coupling to the neighboring Fe LM. These ferromagnetic and antiferromagnetic couplings between Fe LM's produce the spin-glass state (see Fig. 6.) The mechanism mentioned above is based on the nonlinearity of the exchange energy $\Phi_{\mathrm{FeFe}}^{\mathrm{ex}}(\xi)$ and LEE on the amplitude of the LM. Thus the spin-glass state in Fe-Ni alloys belongs to a new type of itinerant-electron spin glass.

The antiferromagnetic coupling of $\Phi_{\mathrm{FeFe}}^{\mathrm{ex}}(\xi)$ does not appear in any value of ξ in the bcc lattice. Thus the ferromagnetism is recovered in the bcc lattice. The Curie temperature in the bcc lattice decreases with increasing Ni concentration. This is not explained by the rigid-band model.

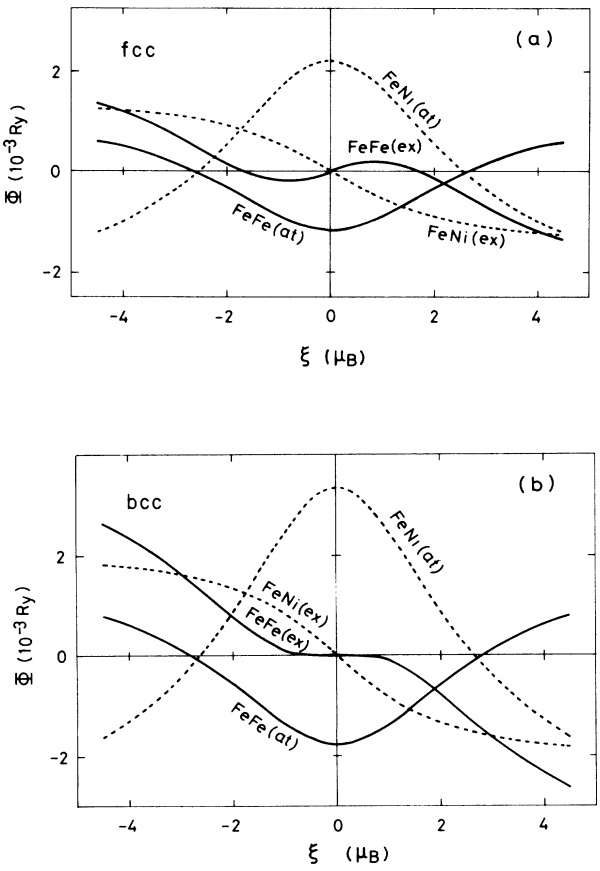

FIG. 5. Pair-energy functionals $\bar{\Phi}_{\alpha\gamma}(\xi)$ and $-\Phi_{\alpha\gamma}^{\mathrm{ex}}(\xi)$ for (a) fcc and (b) bcc $Fe_{65}Ni_{35}$ alloys. They are calculated at $T=900$ K. The notation $\alpha\gamma$(at) [$\alpha\gamma$(ex)] means $\bar{\Phi}_{\alpha\gamma}(\xi)$ $[-\Phi_{\alpha\gamma}^{\mathrm{ex}}(\xi)]$.

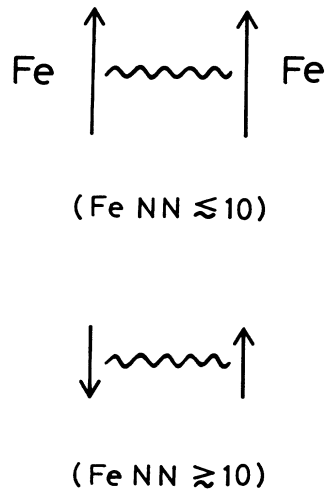

FIG. 6. Nonlinear coupling between Fe LM's in the fcc Fe alloys. Fe LM's with less than ten Fe NN (see Fig. 8) have large amplitudes ($\langle\xi^2\rangle^{1/2}$) and therefore show ferromagnetic coupling, but Fe LM's with more than ten Fe NN have small amplitudes, thus the antiferromagnetic coupling.

IV. LEE IN THE bcc AND fcc LATTICES

A. Concentration dependence

Figure 7 shows the concentration dependence of various LM's. The present choice of parameters shifts the critical concentration of the ferromagnetic instability to the Fe side, resulting in better agreement with the experimental data.[7–9] The amplitudes of the LM $[(\langle m^2\rangle)^{1/2}]$ are enhanced by about 1.5 times for Fe and 3 times for Ni by taking account of the quantum effect. The reduction of the amplitude of Fe LM at c^* is only 7.5%, while it is 16% in the classical expression.[1]

All the average LM in bcc are on the lines extrapolated from the Ni-rich fcc phase. However, the LEE of the bcc phase are considerably different from those in fcc as seen in Fig. 8.

In the fcc lattice, the exchange pair-energy functionals between Fe LM's show the ferromagnetic coupling for the absolute field variable $|\xi| \gtrsim 1.7\mu_B$, and the antiferromagnetic couplings for $|\xi| \lesssim 1.7\mu_B$. The latter couplings become effective when the Fe concentration increases because more atomic pair-energy functionals $\overline{\Phi}_{\mathrm{FeFe}}(\xi)$ act to decrease the amplitude $(\langle\xi^2\rangle)^{1/2}$. The self-consistent treatment of such antiferromagnetic couplings due to LEE leads to the ferromagnetic instability at about $c^* = 65$ at. % Fe in the fcc phase, and to a broad LM distribution near c^*. The ferromagnetic instability and strong LEE on the LM do not take place in the bcc lattice because of no anomaly in $\Phi^{\mathrm{ex}}_{\mathrm{FeFe}}(\xi)$. This is also seen from a comparison of the local DOS of Fe in various environments between the bcc and fcc phases in Fig. 2.

The local-moment distributions for Fe are shown in Fig. 9. The main difference between the previous and present results is that the width of the distribution in the present calculations remains in a small concentration regime after disappearance of the ferromagnetism because of the existence of the spin-glass state. The corresponding internal field distributions seen by ^{57}Fe are shown in Fig. 10. They are consistent with the experimental results by Window.[11] The negative internal fields which imply the existence of the LM antiparallel to the magnetization has recently been verified experimentally by Ullrich and Hesse.[14]

The amplitude distributions for Fe have been calculated by using the new expression (2.17) (see Fig. 11). The widths of the distributions shrink by 50% as compared with the classical results (see Fig. 5(b) in I).

B. Temperature variation

The temperature change of the amplitude of LM is shown in Fig. 12. The amplitudes of Fe are enhanced by

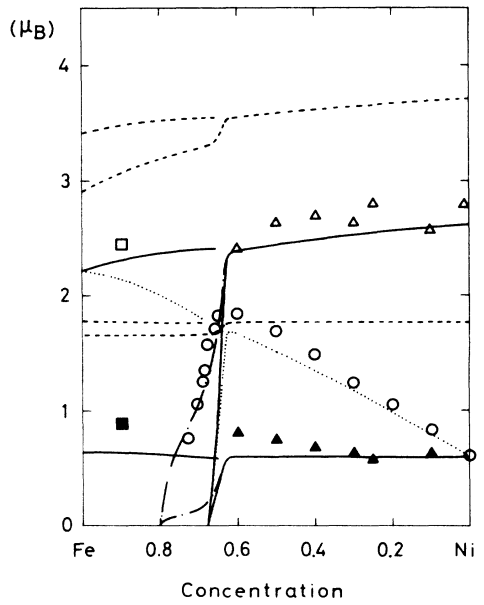

FIG. 7. Concentration dependence of various local moments (LM) in the bcc ($c \geq 0.65$) and fcc ($0 \leq c \leq 1$) structures at $T = 150$ K. (· · · ·): $[\langle m\rangle]_c$; (——): $[\langle m_\alpha\rangle]_c$; (— — —): $[\langle m_\alpha^2\rangle]_c^{1/2}$; (—·—·—·): $[\langle m_\alpha\rangle^2]_c^{1/2}$. Experimental LM $[\langle m_\alpha\rangle]_c$ at $T = 4.2$ K are shown by Δ (α=Fe,fcc), ▲ (α=Ni,fcc) (Refs. 8, 35, and 36), □ (α=Fe,bcc), and ■ (α=Ni, bcc) (Ref. 37). ○ show the experimental data for the magnetization (Refs. 7–9).

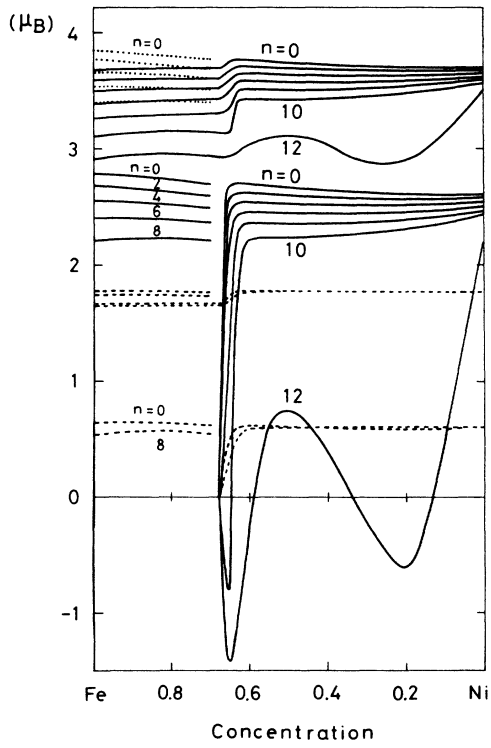

FIG. 8. Average LM $([\langle m_\alpha\rangle_n]_c)$ and the amplitude of LM $([\langle m_\alpha^2\rangle_n]_c^{1/2})$ for Fe (solid curves) and Ni (dashed curves) in various environments at $T = 150$ K. The curves for even numbers of n (the Fe nearest neighbors) are plotted for Fe atoms. For Ni the curves only for $n = 0$ and 8 (or 12) are shown because of weak local environment effects. The amplitude of Fe LM in the bcc phase are drawn by dotted curves to avoid the confusion.

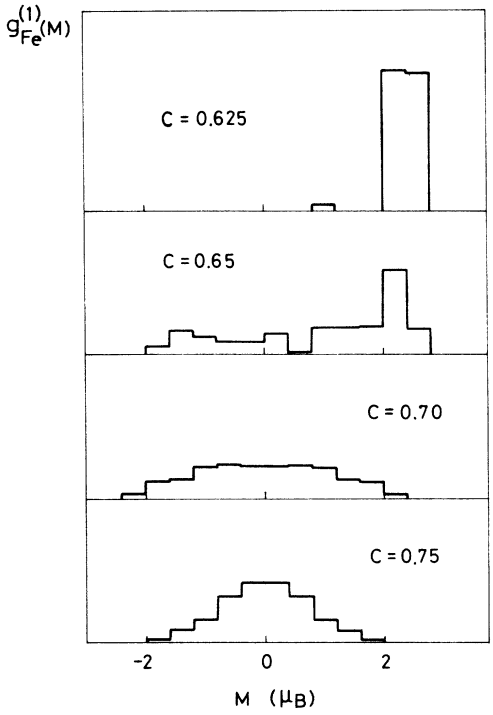

FIG. 9. Distribution functions of Fe LM on the fcc lattice at $T = 150$ K.

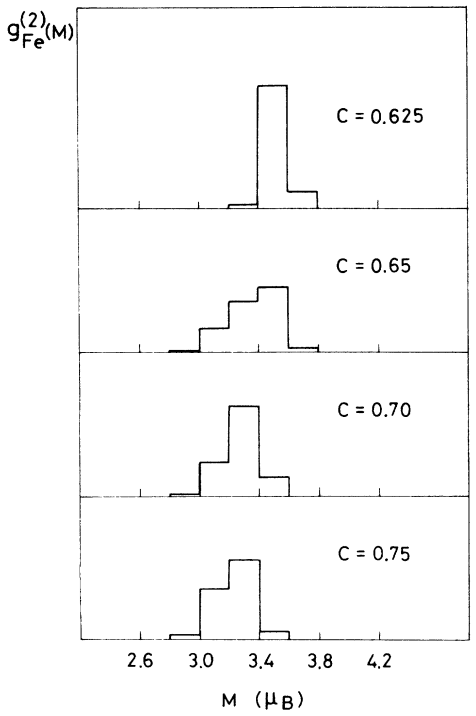

FIG. 11. Calculated distribution functions for the amplitude of Fe LM in various fcc Fe-Ni alloys.

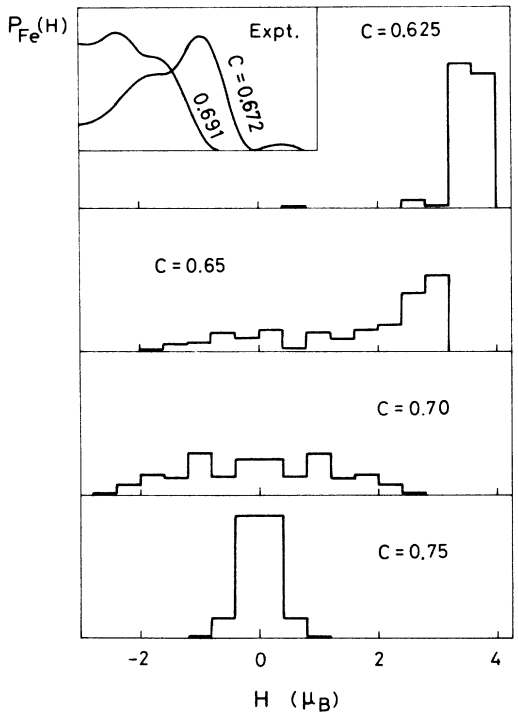

FIG. 10. Internal-field distribution functions relative to ^{57}Fe on the fcc lattice at $T = 150$ K. The inset shows Window's experimental results (Ref. 11) for 67.2 and 69.1 at. % Fe alloys at 300 K.

the quantum effect but the temperature dependence is similar to the previous results.[1] Note that a large change of the amplitude of Fe LM at 60 at. % Fe is responsible for the Invar effect.[19] The Ni LM hardly change the amplitude with increasing temperature in the whole concentrations because of the strong quantum effect.

The temperature change of Fe LM in each environ-

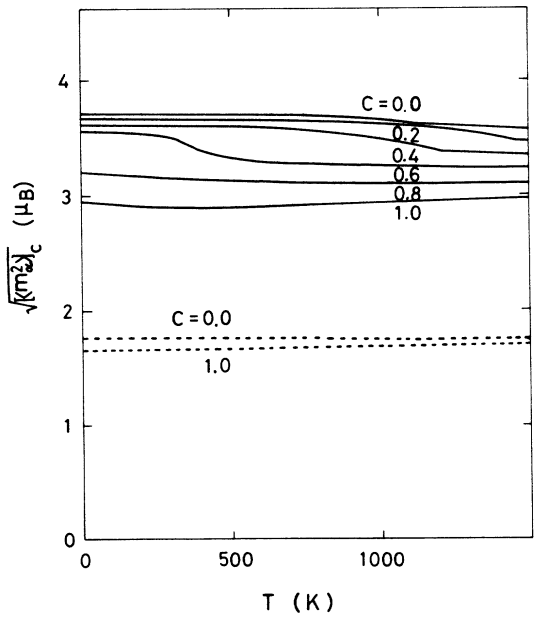

FIG. 12. Amplitude of LM vs temperature curves for Fe (solid curves) and Ni (dashed curves).

ment is shown in Fig. 13 for 62.5 at. % Fe, which is just in the Invar regime. In the previous paper I the results were presented for 50 at. % Fe because of the smaller critical concentration c^*, and therefore the validity of our results was questioned.[38] The new results verify the temperature change near c^* in our previous results; the reversal of Fe LM with ten Fe NN with rising temperature.

The distribution functions of the Fe LM for the same concentration as in Fig. 13 are shown in Fig. 14. The width becomes maximum at $0.6T_c$. The Fe LM antiparallel to the magnetization is clearly seen at finite temperatures. The internal field distribution functions calculated from the LM distributions are presented in Fig. 15. Better agreement with the experimental data[13] is obtained. A peak at $H \approx 0.7\mu_B$ in the distribution functions for $0.53T_c$ and $0.74T_c$ shows the internal fields for the Fe with nine or ten Fe NN, and do not imply the existence of the two γ states suggested by many experimentalists[39,40] and theoreticians.[15,41]

The amplitudes of LM in various environments are depicted in Fig. 13. The use of the new formula enhances the amplitudes and suppresses the temperature change. However, LEE on the amplitude are qualitatively the same as before; the amplitudes of Fe LM with nine or ten Fe NN are considerably reduced with increasing temperature.[1] The widths of the distribution for the amplitude of Fe LM are approximately $0.5\mu_B$ at 62.5 at. % Fe as shown in Fig. 16. They are considerably reduced as compared with the previous results ($\sim 0.7\mu_B$),[1] but the temperature dependence of the line shape is the same as before.

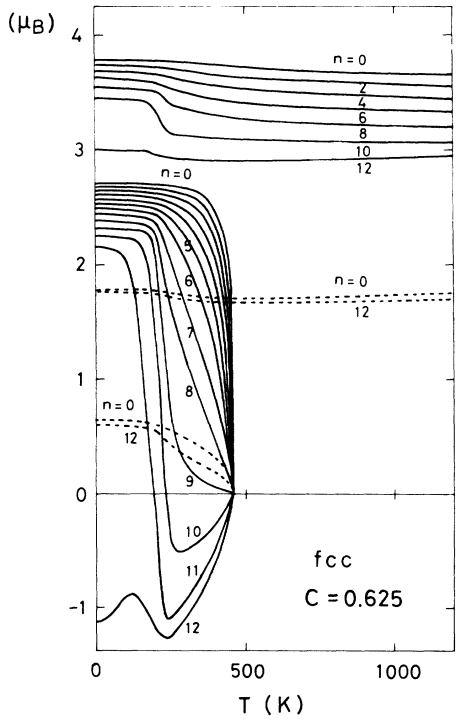

FIG. 13. Temperature dependence of the average LM ($[\langle m_\alpha \rangle_n]_c$) and amplitudes ($[\langle m_\alpha^2 \rangle_n]_c^{1/2}$) for Fe (solid curves) and Ni (dashed curves) atom in various environments.

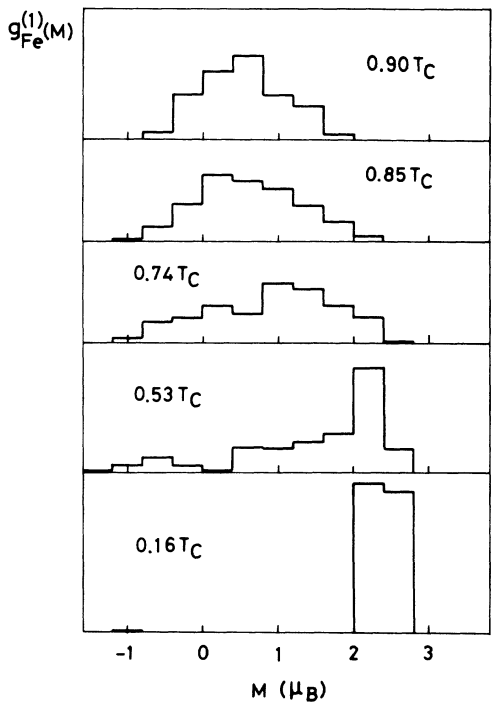

FIG. 14. Temperature dependence of the distribution functions for Fe LM on the fcc lattice at 62.5 at. % Fe.

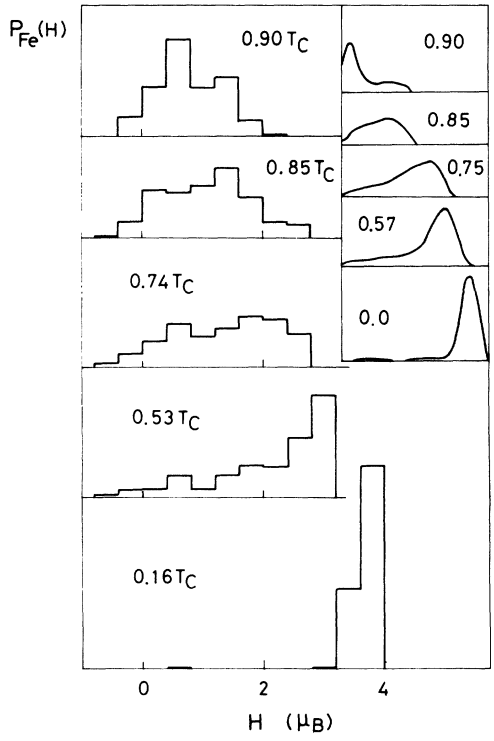

FIG. 15. Temperature dependence of the internal-field distribution functions for ^{57}Fe at 62.5 at. % Fe. The inset shows the experimental results at 65 at. % Fe (Ref. 13).

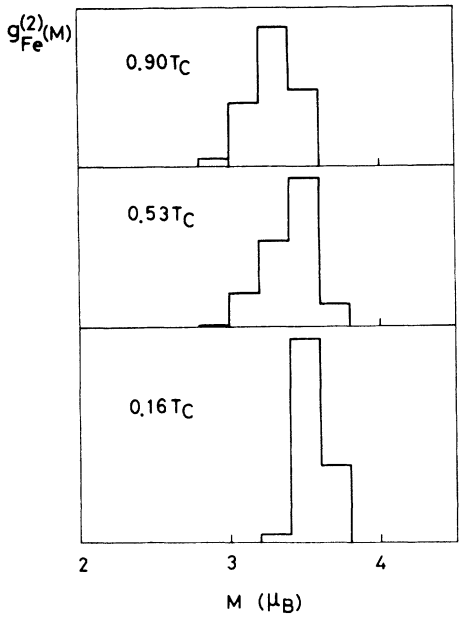

FIG. 16. Temperature variation of the distributions of the amplitude of Fe LM at 62.5 at. % Fe.

V. SUSCEPTIBILITY

The inverse paramagnetic susceptibility versus temperature curves are presented in Fig. 17. The susceptibilities follow the Curie-Weiss law at high temperatures. The curve for γ-Fe deviates from the Curie-Weiss law at low temperatures, and shows a bending at about 300 K. This is related to a minimum in the amplitude $\langle \xi^2 \rangle$ versus temperature curve where the sign of the slope changes. Note that the Curie constant in the weak ferromagnetic case is given by $C = \langle \xi^2 \rangle (1 + a \partial \langle \xi^2 \rangle / \partial T)$ (see Ref. 42). The constant a is determined by a given band structure. The cusp for 75 and 80 at. % Fe curves shows the spin-glass phase transition.

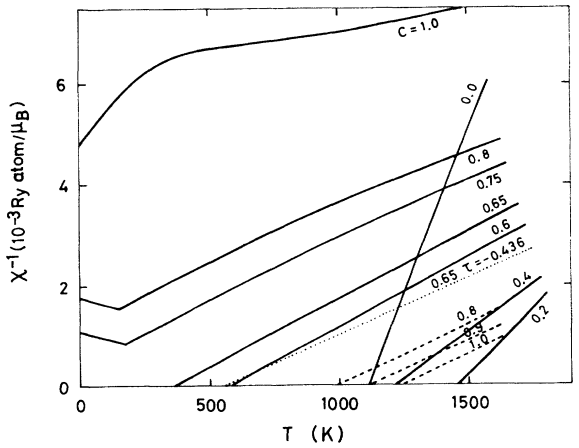

FIG. 17. Paramagnetic susceptibility vs temperature curves in the fcc (solid curves) and bcc (dashed curves) structures. Numerals in the figure show the Fe concentration. Dotted curve shows the result for $Fe_{65}Ni_{35}$ with the atomic short-range order $\tau = -0.436$.

The effective Bohr magneton numbers and the Weiss constants are presented for both bcc and fcc lattices in Fig. 18. The results are in good agreement with the experiments[43–46] and previous results of the CPA calculations.[47,48] The difference of the effective Bohr magneton number m_{eff} between fcc and bcc alloys arises at more than 70 at. % Fe where the fcc ferromagnetism disappears. The calculated m_{eff} of α Fe is $2.8\mu_B$, while it is $4.6\mu_B$ for γ Fe. This indicates a weak magnetism of γ-Fe.[49]

The susceptibility for the 65 at. % Fe alloys with the atomic short-range order $\tau = -0.436$ which leads to the lowest probability p_a^{NiNi} on the fcc lattice is also shown in Fig. 17 by a dotted curve. Since $\mathcal{J}_{\text{FeNi}} > \mathcal{J}_{\text{FeFe}}$ and $\mathcal{J}_{\text{NiFe}} > \mathcal{J}_{\text{NiNi}}$, the Curie temperature is larger than that in the complete random alloys. The effective Bohr magneton number for $\tau = -0.436$ is larger than that in the complete random alloys because the Fe LM are more localized in the environment with the larger number of Ni NN.

A typical example of LEE on the susceptibilities near the ferromagnetic instability is depicted in Fig. 19. The Fe LM with more than ten Fe NN do not follow the Curie-Weiss law. The negative divergence of these Fe LM is due to the antiferromagnetic couplings with surrounding Fe LM's.

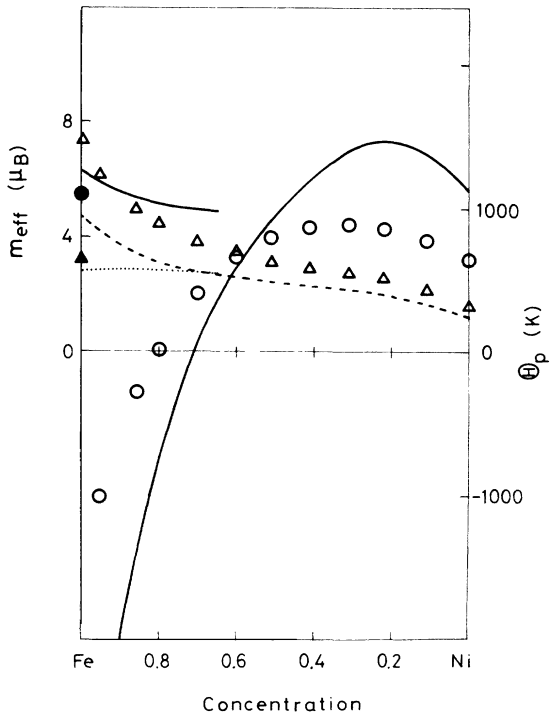

FIG. 18. Concentration dependence of the effective Bohr magneton number m_{eff} (dotted and dashed curves) and the Weiss constant (solid curves) for the bcc ($c \geq 0.65$) and fcc structures. The results are obtained at about 1300 K. Open (closed) triangles and circles show the experimental m_{eff} and Weiss constants, respectively, for the fcc (Refs. 43 and 44) (bcc) (Refs. 45 and 46) structure.

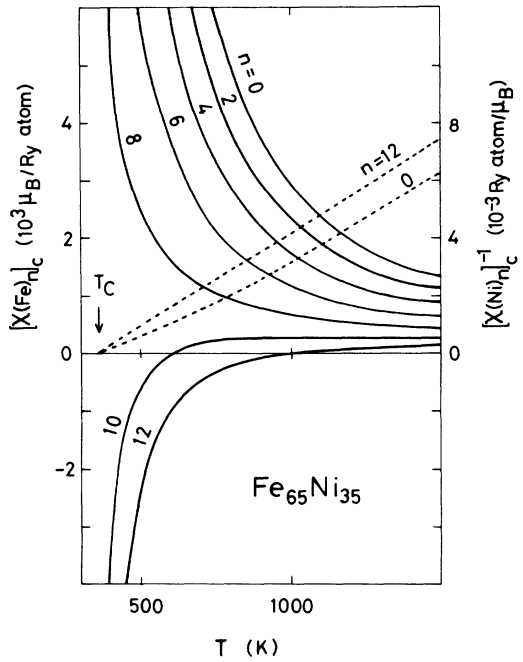

FIG. 19. Paramagnetic susceptibilities of Fe (solid curves) and Ni (dashed curves) atoms in various environments for 65 at. % Fe fcc alloys.

The calculated high-field susceptibilities at low temperatures are shown in Fig. 19 as a function of the concentration. When we approach to the critical concentration from the lower Fe concentration the calculated susceptibilities rapidly increase. But the rate of the increment is too large as compared with the experiments.[50] One has to take into account more seriously the electron correlations there. When the ferromagnetism disappears, the amplitude of Fe LM shrink considerably as has been shown in Fig. 8. The Fe LM with eight and nine Fe NN hardly feel the molecular fields from the surrounding Fe LM via the exchange coupling $\Phi^{ex}_{FeFe}(\xi)$ because of the reduction of the amplitude [see Fig. 3(a)]. This causes relatively large susceptibilities in the paramagnetic and spin-glass phase as seen in Fig. 20. Therefore, an asymmetric divergence of susceptibility arises around the critical concentration in the fcc phase. Unfortunately there is no experimental data available at more than 70 at. % Fe.

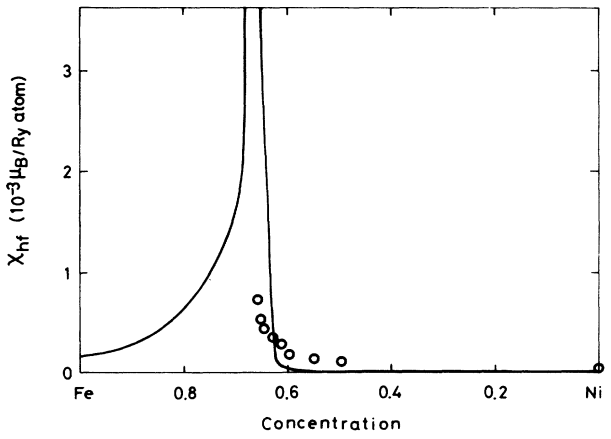

FIG. 20. High-field susceptibility as a function of the Fe concentration at $T=150$ K. Open circles show the experimental results at 4.2 K (Refs. 50 and 51).

VI. SUMMARY

In the present paper we have investigated the finite-temperature magnetism of Fe-Ni alloys in both bcc and fcc structures on the basis of the theory of LEE.

The bcc and fcc magnetic phase diagrams explain well the experimental ones. The decrease of the Curie temperature with increasing average electron numbers in the bcc phase[30] has been shown to be due to the alloying effect. In the fcc structure we have given theoretical support to the spin-glass state which has quite recently been found experimentally by Takahashi *et al.*[20,21] Calculated susceptibilities show a cusp at the transition temperatures. This spin-glass state is purely itinerant in the sense that it does not occur unless we take account of the nonlinearity of the magnetic coupling between Fe LM and LEE on the amplitude of Fe LM. These characteristics seem to be quite general in the close-packed Fe alloys. We speculate therefore that the spin-glass states in amorphous Fe-Zr and Fe-La alloys,[31,32] which have recently been found, might be explained by the same mechanism. It is quite interesting to clarify in experimental and theoretical investigations what are the characteristics which distinguish itinerant-electron spin glasses from insulator spin glasses.

As we have shown in the previous paper (I), the key to understanding the magnetism of Fe-Ni alloys is the nonlinearity with respect to the atomic configuration of the couplings between Fe LM's via the amplitude fluctuations. This explains the rapid decrease of the magnetization near c^*, and the temperature and concentration dependence of the internal-field distributions acting on ^{57}Fe. In the present calculations we have checked our previous conclusions,[1] and have obtained better agreement with experiments by using more reasonable input parameters.

We have taken into account the quantum effect on the amplitude of LM by using a new expression[18] consistent with the free energy. The amplitudes of LM are enhanced by a factor of 1.5 for Fe and 3.0 for Ni as compared with the previous results. The temperature and concentration dependencies of the amplitude are suppressed by the quantum effect; the amplitude reduction at T_c is only 4.5% at 60 at. % Fe and the amplitude change at c^* is only 6.5% at low temperatures.

The effective Bohr magneton numbers m_{eff} and the Weiss constants Θ_p in the paramagnetic susceptibilities were shown to be consistent with the experiment; the calculated m_{eff} in the fcc structure increase rapidly near c^* while those in the bcc hardly change in the Fe-rich concentrations. One of our predictions is that the high-field susceptibility shows an asymmetric divergence around c^* in the fcc structure. This asymmetry is caused by the Fe LM's with eight Fe NN, which have very small exchange

coupling in the paramagnetic state. It might be possible to verify the asymmetric dependence by investigating $(Fe_cNi_{1-c})_{92}C_8$, $(Fe_{0.65}Ni_{0.35})_{1-c}Mn_c$ alloys,[21,52] and Fe-Zr[31] Fe-La,[32] and $(Fe_{1-c}Ni_c)_{75}P_{16}B_6Al_3$ amorphous alloys.[53]

Finally we note that we did not discuss the so-called Invar problems. The static approximation with reduced Coulomb and exchange-energy parameters, which has been used in the present calculations, describes qualitatively well $\langle m_\alpha \rangle$ and x_α.[54] It also explains the large negative thermal-expansion coefficient[19] and large forced volume magnetostriction[48] near c^*, but it does not describe the change of sign as a function of concentration in these quantities.[19,48] Furthermore, one has to assume a volume dependence of the effective exchange energy parameter in order to explain the pressure dependence of T_c $(\partial T_c/\partial P)$ versus concentration curves.[48] One has to take account of the electron correlations at finite temperatures to consistently discuss the Invar phenomena on the basis of a microscopic theory.[55] This is one of the important problems in Fe-Ni alloys, which needs to be addressed in the future.

ACKNOWLEDGMENT

The author would like to thank Dr. V. L. Moruzzi for valuable discussions on the DOS used in the present paper during his stay at IBM Yorktown Heights.

[1]Y. Kakehashi, J. Magn. Magn. Mater. **37**, 189 (1983).
[2]F. Matsubara, Prog. Theor. Phys. **52**, 1124 (1974).
[3]S. Katsura, S. Fujiki, and S. Inawashiro, J. Phys. C **12**, 2839 (1979).
[4]R. L. Stratonovich, Dokl. Akad. Nauk. SSSR **115**, 1097 (1958) [Sov. Phys.—Dokl. **2**, 416 (1958)].
[5]J. Hubbard, Phys. Rev. Lett. **3**, 77 (1959).
[6]S. Q. Wang, W. E. Evenson, and J. R. Schrieffer, J. Appl. Phys. **41**, 1199 (1970).
[7]J. Crangle and G. C. Hallam, Proc. R. Soc. London **272**, 119 (1963).
[8]M. F. Collins, R. V. Jones, and R. D. Lowde, J. Phys. Soc. Jpn. **17**, 19 (1962).
[9]Y. Bando, J. Phys. Soc. Jpn. **19**, 237 (1964).
[10]H. Rechenberg, L. Billiard, A. Chambered, and N. Natta, J. Phys. Chem. Solid **34**, 1251 (1973).
[11]B. Window, J. Appl. Phys. **44**, 2853 (1973).
[12]U. Gonser, S. Nasu, and W. Kappes, J. Magn. Magn. Mater. **10**, 244 (1979).
[13]M. Shiga and Y. Nakamura, J. Magn. Magn. Mater. **40**, 319 (1984).
[14]H. Ullrich and J. Hesse, J. Magn. Magn. Mater. **45**, 315 (1984).
[15]A. R. Williams, V. L. Moruzzi, C. D. Gellatt, Jr., and J. Kübler, J. Magn. Magn. Mater. **31 - 34**, 88 (1983).
[16]D. D. Johnson, F. J. Pinski, and G. M. Stocks, J. Phys. **57**, 3018 (1985).
[17]H. Hasegawa, J. Phys. F **13**, 1915 (1983).
[18]Y. Kakehashi, Phys. Rev. B **34**, 3243 (1986).
[19]Y. Kakehashi, J. Phys. Soc. Jpn. **50**, 2236 (1981).
[20]T. Miyazaki, Y. Ando, and M. Takahashi, J. Magn. Magn. Mater. **60**, 219 (1986); **60**, 227 (1986).
[21]S. Ishio, K. Nushiro, and M. Takahashi, J. Phys. F **16**, 1093 (1986).
[22]J. A. Hertz, Phys. Rev. B **19**, 4776 (1979); in *Electron Correlation and Magnetism in Narrow-Band Systems,* edited by T. Moriya (Springer-Verlag, Berlin, 1981), p. 138.
[23]Y. Kakehashi, Phys. Rev. B **35**, 4973 (1987).
[24]Y. Kakehashi, J. Magn. Magn. Mater. **66**, L163 (1987).
[25]Y. Kakehashi, Phys. Rev. B **32**, 3025 (1985).
[26]H. Danan, A. Herr, and A. J. P. Meyer, J. Appl. Phys. **39**, 669 (1968).
[27]D. D. Johnson, B. L. Gyorffy, P. J. Pinski, J. Staunton, and G. M. Stocks (unpublished).
[28]P. W. Anderson, Phys. Rev. **115**, 2 (1959).
[29]M. Lacour-Gayet and M. Cyrot, J. Phys. C **1**, 400 (1974).
[30]R. M. Bozorth, *Ferromagnetism* (Van Nostrand, Princeton, 1968), p. 102.
[31]N. Saito, H. Hiroyoshi, K. Fukamichi, and Y. Nakagawa, J. Phys. F **16**, 911 (1986).
[32]H. Wakabayashi, K. Fukamichi, H. Komatsu, T. Goto, T. Sakakibara, and K. Kuroda (unpublished).
[33]Y. Kakehashi, J. Phys. Soc. Jpn. **50**, 3177 (1981); **52**, 637 (1983).
[34]Y. Kakehashi, J. Magn. Magn. Mater. **43**, 79 (1984).
[35]C. G. Shull and M. K. Wilkinson, Phys. Rev. **97**, 304 (1955).
[36]M. F. Collins and G. G. Low, Proc. Phys. Soc. London **86**, 535 (1965).
[37]M. F. Collins and J. B. Forsyth, Philos. Mag. **8**, 401 (1963).
[38]E. P. Wohlfarth (private communication).
[39]R. J. Weiss, Proc. Phys. Soc. London **82**, 28 (1963).
[40]S. Chikazumi, J. Magn. Magn. Mater. **15 - 18**, 1130 (1980).
[41]D. M. Roy and D. G. Pettifor, J. Phys. F **7**, L183 (1977).
[42]H. Hasegawa, J. Phys. Soc. Jpn. **49**, 178 (1980).
[43]Y. Nakagawa, J. Phys. Soc. Jpn. **12**, 700 (1957).
[44]V. I. Chechernikov, Zh. Eksp. Teor. Fiz. **42**, 956 (1962) [Sov. Phys.—JETP **15**, 659 (1962)].
[45]W. Sucksmith and R. R. Pearce, Proc. R. Soc. London, Ser. A **167**, 189 (1938).
[46]M. Fallot, J. Phys. Rad. **V**, 153 (1944).
[47]H. Hasegawa, in *Electron Correction and Magnetism in Narrow-Band Systems,* edited by T. Moriya (Springer-Verlag, Berlin, 1981), p. 38.
[48]Y. Kakehashi, J. Phys. Soc. Jpn. **51**, 3183 (1982).
[49]P. Rhodes and E. P. Wohlfarth, Proc. R. Soc. London, Ser. A **273**, 427 (1963).
[50]I. Nakai, F. Ono, and O. Yamada, J. Phys. Soc. Jpn. **52**, 1791 (1983).
[51]J. P. Rebouillat, TEEE Trans. Magnet. Mag. **8**, 630 (1972).
[52]M. Shiga, T. Satake, Y. Wada, and Y. Nakamura, J. Magn. Magn. Mater. **51**, 123 (1985).
[53]Y. Yeshurum, M. B. Salamon, K. V. Rao, and H. S. Chen, Phys. Rev. B **24**, 1536 (1981).
[54]Y. Kakehashi and P. Fulde, Phys. Rev. B **32**, 1595 (1985).
[55]Y. Kakehashi and J. H. Samson, Phys. Rev. B **34**, 1734 (1986).